analytical chemistry

Article

Label-free TOF-SIMS imaging of sulfur producing enzymes inside microglia cells following exposure to silver nanowires

Bey Fen Leo, Sarah Fearn, Daniel Gonzalez-Carter, Ioannis Theodorou, Pakatip Ruenraroengsak, Angela Goode, David Mcphail, David T. Dexter, Milo Sebastian Peter Shaffer, Kian Fan Chung, Alexandra E Porter, and Mary P. Ryan

Anal. Chem., **Just Accepted Manuscript** • DOI: 10.1021/acs.analchem.9b01704 • Publication Date (Web): 16 Jul 2019

Label-free TOF-SIMS imaging of sulfur producing enzymes inside microglia cells following exposure to silver nanowires

Bey F. Leo[1,2], Sarah Fearn[1], Daniel Gonzalez-Cater[3], Ioannis Theodorou[1], Pakatip Ruenraroengsak[1], Angela E. Goode[1], David McPhail[1], David T. Dexter[3], Milo Shaffer[1,4], Kian F. Chung[5], Alexandra E. Porter[1] and Mary P. Ryan[1]**

[1]Department of Materials and London Centre for Nanotechnology, Imperial College London, Exhibition Road, London, UK, SW7 2AZ

[2]Central Unit for Advanced Research Imaging (CENTUARI), Faculty of Medicine, University of Malaya 50603 Kuala Lumpur

[3]Innovation Center of NanonMedicine, 3 Chome-25-14, Tonomachi, Kawasaki, Japan 210-0821

[4]Department of Chemistry and London Centre for Nanotechnology, Imperial College London, Exhibition Road, London, UK, SW7 2AZ

[5] Experimental Studies, National Heart & Lung Institute, Imperial College London, London SW3 6LY

KEYWORDS. Silver nanomaterials, TOF-SIMS, enzymes, microglial cells

Abstract

There are no methods sensitive enough to detect enzymes within cells, without the use of analyte labelling. Here we show that it is possible to detect protein ion signals of three different H_2S-synthesizing enzymes inside microglia after pre-treatment with silver nanowires (AgNW) using time of flight-secondary ion mass spectrometry (TOF-SIMS). Protein fragment ions, including the fragment of amino acid ($C_4H_8N^+$ - 70 amu), fragments of the sulfur producing cystathionine-containing enzymes and the Ag^+ ion signal could be detected without the use of any labels; the cells were mapped using the $C_4H_8N^+$ amino acid fragment. Scanning electron microscopy imaging and energy dispersive x-ray chemical analysis showed that the AgNWs were inside the same cells imaged by TOF-SIMS and transformed chemically into crystalline Ag_2S within cells in which the sulfur producing proteins were detected. The presence of these sulfur producing cystathionine-containing enzymes within the cells was confirmed by Western Blots and confocal microscopy images of fluorescently labelled antibodies against the sulfur producing enzymes. Label-free ToF-SIMS is very promising for the label-free identification of H_2S-contributing enzymes and their cellular localization in biological systems. The technique could in future be used to identify which of these enzymes are most contributory.

Introduction

New insights into the function and activity of biological systems, from the toxicity of nanomaterials to the role of misfolded proteins in disease, require not only the identification of the proteins and nanomaterials, but also knowledge of their localisation and chemistry within complex biological assemblies. This characterisation must relate the spatial distribution of the proteins or particles of interest to their cellular surroundings. Traditionally analyte labelling (e.g. with fluorescent dyes or radioisotopes) is used to image the distribution of protein or enzymes, however a limitation of fluorescence microscopy is that it relies on a prior knowledge of which proteins are present in a specific tissue; in addition the spatial resolution of this technique is diffraction-limited. Super resolution light microscopy surpasses the diffraction limit and is a very powerful tool for imaging proteins inside cells[1], nevertheless advanced knowledge of which proteins are present is still required.

An alternative method for spatially resolved, label-free surface analysis of enzymes and proteins within cells is time of flight-secondary ion mass spectrometry (TOF-SIMS). In TOF-SIMS, the sample surface is bombarded by an energetic focused primary ion beam leading to the ejection of secondary ions. The energy of the primary ion beam will vary depend on the instrumentation used and may be as low as sub-keV or as high as MeV. These ions (positive or negative) are accelerated by a potential of 2000 V into the flight tube. The ions, which all now possess the same kinetic energy (KE), are allowed to drift through a field-free flight tube, of length L, until striking a detector. As the ions all have the same kinetic energy, the time taken for the ions to strike the detector determines their mass, and the mass to charge ratio (m/z) can be accurately determined. TOF-SIMS spectra are calibrated internally using low mass fragment ions with a mass accuracy within a typical range of 10-100 ppm. Mass spectra with high mass resolution and chemical maps with sub-micron spatial resolution are produced by rastering the ion beam across the sample surface. This technique can provide mass spectra resolving the fragments of amino acids contained in proteins, as well as elemental metal ion maps with high sensitivity[2]. As the analyte remains in its solid state, chemico-spatial information can be obtained, and importantly, if the ToF-SIMS analysis is carried out under static conditions, *i.e.* the ion beam fluence is low and no beam damage occurs to the sample, the same area can be correlated with complementary techniques, such as scanning electron microscopy (SEM) or confocal microscopy.

In previous work, TOF-SIMS spectra have been acquired indirectly from enzymes, using calcium as their co-factor in ischemic retinal tissue [3]. The activity of enzymes in biomass has also been detected by TOF-SIMS to analyse the relative abundance of polysaccharides and lignin at the biomass surface during the degradation process [4, 5]. Both organic and metallic species can be investigated simultaneously, with high spatial resolution (up to 200 nm) [6]. Other work has used ToF-SIMS to map the differences in the distribution of lipid and amino acid profiles on the mucosal surface of normal and inflamed tissues of biopsy specimens in patients with ulcerative colitis and dysplasia [7]. This technique has also been used to map biochemically distinct regions in breast cancer tissues pre- and post- chemotherapy by mapping differences in molecules, such as fatty acids and Vitamin E [8]. Nevertheless, none of these previous studies mapped enzymes in the cellular environment using their fragment ions. Analyte labelling (e.g. with fluorescent dyes or radioisotopes) is commonly used to image the distribution of protein or enzymes. Label-free imaging of enzymes, introduced in this study, may offer an alternative approach, for instance effective probes need not be developed for each analyte, nor must the system be perturbed by the introduction of exogenous compounds, and parallel imaging of multiple analytes is not limited by the number of simultaneously usable or detectable probes.

Using a system that is an interesting exemplar of a system that is controlled by local enzyme regulation, this study aimed to show that fragments of amino acids from sulfur-producing enzymes could be detected and quantified using TOF-SIMS inside individual microglia - the resident macrophages of the central nervous system [9] - after pre-treatment with silver nanowires (AgNWs). Our recent study examined the *in vitro* uptake and intracellular transformation of spherical silver nanoparticles (AgNPs) inside microglia and showed, using confocal microscopy, that these AgNPs are transformed into insoluble Ag_2S NPs by upregulation of H_2S – synthesizing enzyme cystathionine-γ-lyase (CSE) [9], which has been shown to exert neuroprotection through its anti-inflammatory effects [10, 11]. This study has significance in the field of nanotoxicology, where unintentional inhalation of these nanostructures, following their release into the environment, could cause neurotoxicity if they translocate inside the brain.

RESULTS

Figure 1(a) shows the initial SIMS analysis of the control microglial cells (no Ag exposure) deposited onto a silicon wafer. In both of the ion images of figure 1(a) representing the secondary ions of protein and cystathionine fragments, no clear ion image was obtained as the surface of the samples are highly contaminated. In order to improve the secondary ion intensity and signal to noise ratio of the secondary ion signals, the samples were sputter cleaned with the C_{60}^+ cluster ion beam. The same secondary ions collected in figure 1(a) are now clearly resolved in figure 1(b). The NH_4^+ at 18.0350 amu (dev. +53.9ppm), $C_4H_8N^+$ at 70.0668 amu (dev. +23.5ppm) and $C_5H_{12}N^+$ at 86.1004 amu (dev. +86.1004ppm) secondary ions were used for identification of cells, originating from the fragmentation of proteins [12]; whereas a number of fragment ions were used to identify the cystathionine (Cys), and are listed in table 1 [13]. The sputter clean removes the surface contaminants, such as polydimethylsiloxane (PDMS), which is commonly observed on the surface of biological samples during SIMS analysis [14]. To avoid this contamination, the resin embedded microglia used in this study should be stored in cardboard boxes in future studies. The presence of PDMS on the sample surface acts to suppress the secondary ion counts of interest.

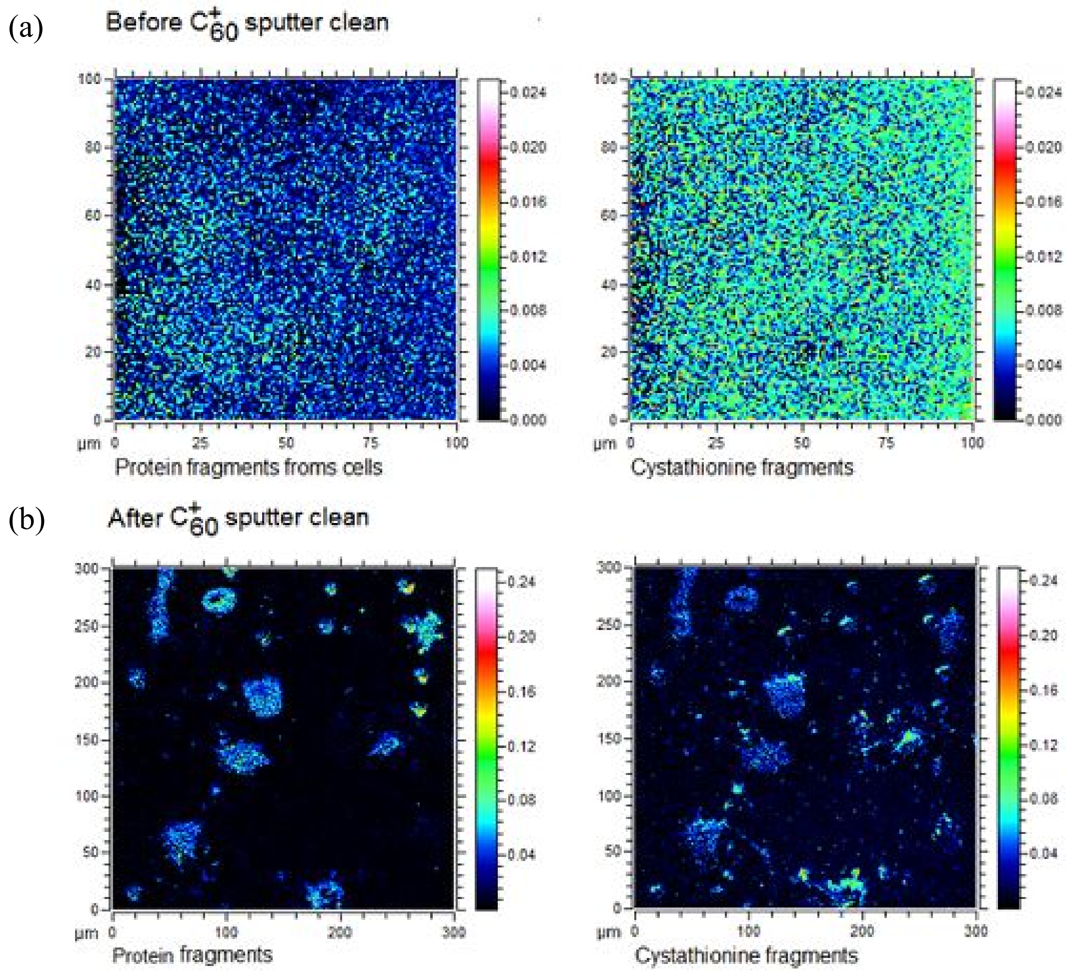

Fig. 1: *TOF-SIMS images of control microglia cells: (a) Before C_{60}^+ sputtering showing a contaminant layer on the surface of the samples and (b) after C_{60}^+ sputtering. NH_4^+, $C_4H_8N^+$ and $C_5H_{12}N^+$ were used for*

identification of cells. The cystathionine fragments identified and used for the ion image are listed in table 1 below.

Molecular structure of cystathionine ($C_7H_{14}N_2O_4S$, 222 amu).

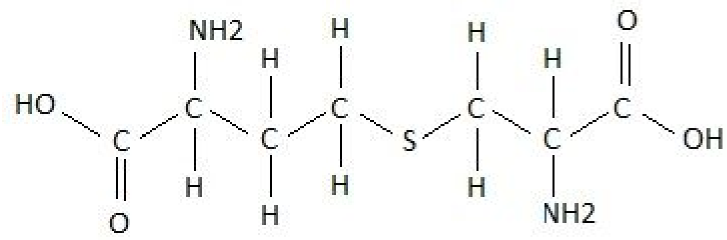

Table 1 *– Cystathionine molecular structure, and the secondary ion fragments identified from the high resolution mass spectra.*

Cystathionine	Mass	deviation (ppm)
CH_3N^+	29.0256	-11.2
CHO_2^+	44.9960	-29.8
$C_4H_7NO^+$	85.0512	-17.9
$C_3H_6NO_2^+$	88.0400	+3.8
$C_4H_8NO_2^+$	102.0559	+4.9
$C_6H_{13}N_2O_2^+$	145.0898	-39.7
$C_7H_{10}SO_4^+$	190.0140	-73.9
$C_7H_{13}SN_2O_3^+$	205.0643	-41.5
$C_6H_{13}SN_2O_4^+$	209.0394	-94.8
$C_7H_{14}SN_2O_4^+$	222.1166	+22.0

TOF-SIMS analysis: Cellular uptake of the AgNWs in microglial cells after C_{60}^+ sputtering

To detect sulfur-producing enzymes by N9 microglial cells *and* cellular uptake of the AgNWs, the TOF-SIMS images were correlated with high resolution FIB-SEM images. Positive secondary ion signals were collected using high-mass-resolution mode (m/Δm ~7000), TOF-SIMS data identified both the presence of Ag^+ and ion fragments related to the sulfur-producing enzymes (Figure 2). The secondary ion intensities were higher for positive ions compared to those obtained for the negative secondary ion collection (Figure S1). Ag^+ ion peaks were clearly seen in the positive ion spectrum in the cells containing the AgNWs. Figure 3 highlights that the

Ag signals were much lower in the control sample (Figure 3(a), (b), (c)) than in the Ag exposed samples, where two peaks at 106.9 amu and 108.9 amu represent $^{107}Ag^+$ and $^{109}Ag^+$, respectively (Figure 3(d), (e)). The isotope ratio for the two peak was measured and found to be 52.01% for the Ag and 47.99% for the 109Ag. Moreover, protein fragment ion signals, including the amino acids ($C_4H_8N^+$ at 70 amu), and the cystathionine fragments were clearly observed in the mass spectra. Peak assignments for the protein fragment ions were confirmed by comparison with reference spectra recorded at high mass resolution with epithelial like cells [15]. These signals were detected in cells with, and without exposure to the AgNWs, which is expected as they are biologically present in the cells [9, 10]. However, no quantifiable and systematic change in the signals were observed between the two sets of cells, indicating no upregulation of the enzyme in the cells exposed to AgNWs was detected in the SIMS signal. The fragmented groups from the cystathionine molecule produced the most readily identifiable peaks on the mass spectra, therefore, these signals were selected as representative secondary ion fragments of the enzymes for subsequent SIMS ion imaging and correlation to the SEM analyses. The Ag^+ ions peaks were clearly observed in the ion spectrum of AgNW-treated microglia cells samples (Figure 2b), but not in the controls (Figure 2a). This difference is also highlighted in figure 3.

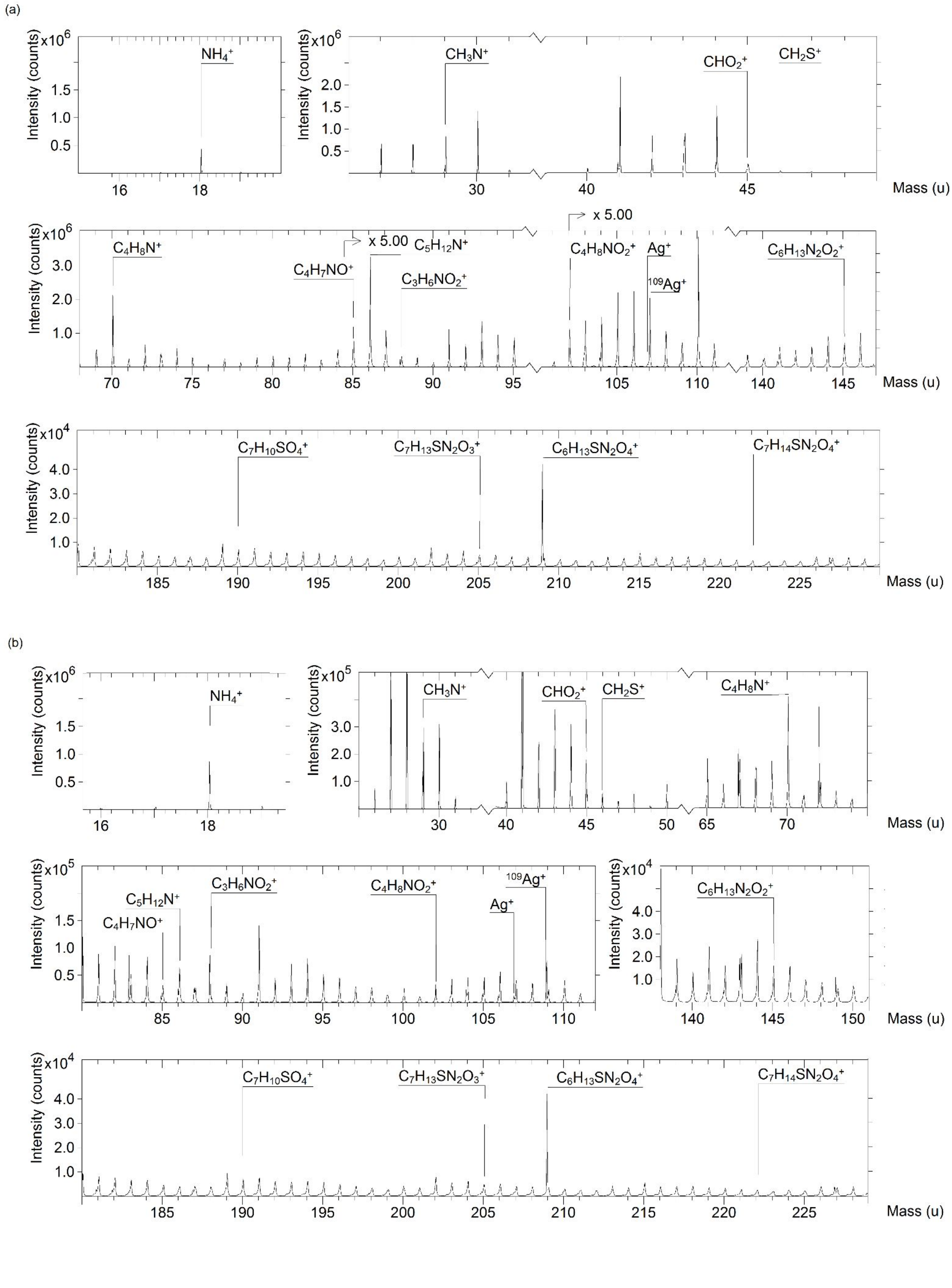
(a)
Intensity (counts)
x10^6
NH4+
CH3N+
CHO2+
CH2S+
Mass (u)
C4H8N+
C4H7NO+
x 5.00
C5H12N+
C3H6NO2+
C4H8NO2+
Ag+
109Ag+
C6H13N2O2+
x10^4
C7H10SO4+
C7H13SN2O3+
C6H13SN2O4+
C7H14SN2O4+
(b)
x10^5

Figure 2: *(a) Secondary-ion mass spectrum (positive polarity) obtained from control (NA) microglial cells with no Ag, after sputtering with C_{60}^{+}, showing that a signal from the sulfur-rich enzymes can be detected above the signal to noise ratio (SNR). (b) Secondary-ion mass spectrum (positive polarity) recorded from microglia cells exposed to AgNWs for 24 hours at a concentration of 50 µg/ml after sputtering with C_{60}^{+}, showing that it is possible to detect the Ag^{+} ion peak and cysteine containing protein fragment ions above the signal to noise ratio.*

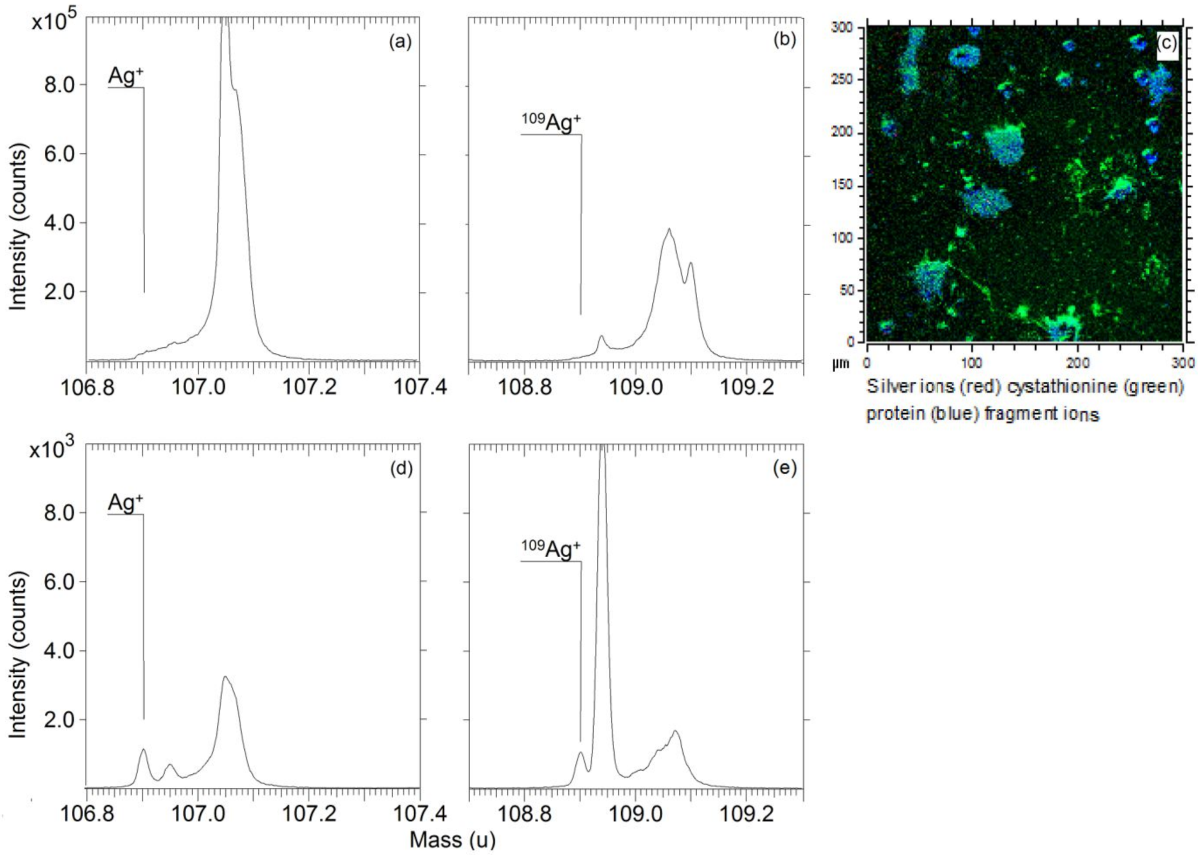

Figure 3*: (a) and (b) show the mass spectra obtained from control (NA) microglial cells indicating that no Ag^{+} ions can be observed in the control sample; (c) the corresponding ion image from the control microglial cells. (d) and (e) show mass spectra obtained from the AgNW exposed microglial cells indicating that the Ag^{+} ions can be detected in the cells exposed to AgNWs.*

Secondary ion maps of the N9 microglial cells containing AgNWs (Figure 4a-d) were successfully correlated with SEM images of the same region (Figure 4e). The protein fragment ion $C_4H_8N^+$ was clearly detected and could be used to define same cell regions in the SEM and SIMS images. The AgNWs are clearly visible in the BSE-SEM image (Figure 4e) due to their high electron density; high Ag^{+} secondary ion intensity was identified in these same locations (Figure 4c) showing that the TOF-SIMS images can locate the AgNWs successfully and the results were reproducible. To establish whether it was possible to map the sulfur-producing enzymes in the cells exposed to AgNWs, the fragments identified in the high resolution mass spectra (Figure 2b) were additionally mapped within the N9 microglial cells exposed to the AgNWs (Figure 4b and d and Figure SI2).

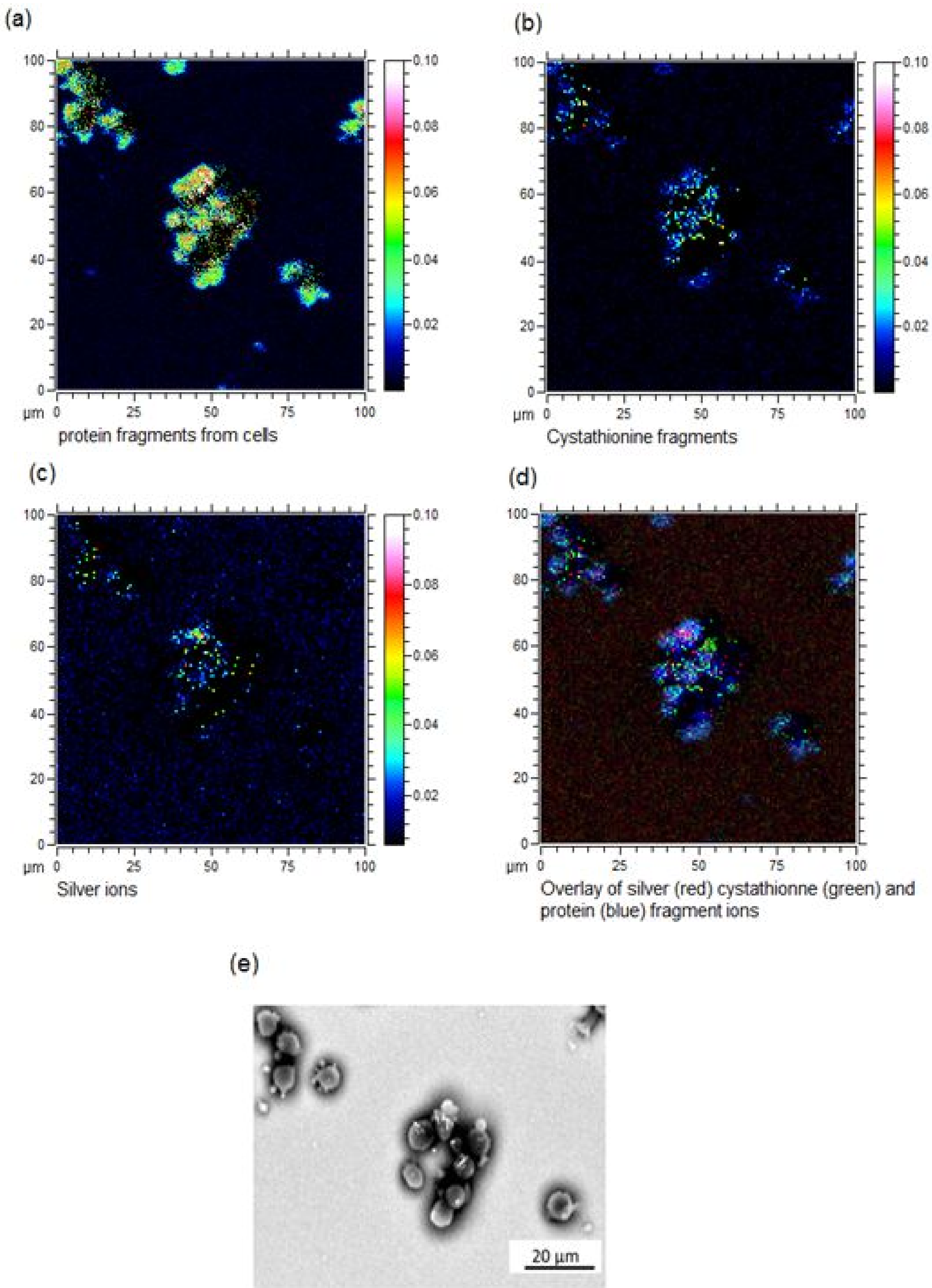

Figure 4: *(a) TOF-SIMS surface ion maps of the same cells and (e) SEM of microglial cells exposed to silver nanowires (D=70 nm, L= 1 - 4 µm, C=50µg/ml) for 24 hours. Red: Ag, Green: Cystathionine fragments ($C_6H_{13}N_2O_4S^+$). Blue: Protein fragment ion ($C_4H_8N^+$).*

ToF-SIMS is a versatile technique, as it is possible to identify and measure both organic and inorganic species at the same time, with a high spatial resolution capability up to 200 nm, depending on the secondary ion signal. Although SIMS operated in imaging mode has been shown to detect certain groups of molecules, such as lipids at the nanometer scale and at attomolar concentration[16], this technique is less sensitive to large molecules with high mass to charge ratios (m/z ≥ 1000) .

FIB cross-sectioning of cell samples

After the same group of cells had been co-located by both SEM imaging and TOF-SIMS surface ion mapping (Figure 4), the same cell-region was cross-sectioned with a Ga^+ focused ion beam (FIB) to expose their internal structure. The preservation of the three-dimensional shape of the cells is clear in the side-view secondary electron images obtain in the FIB instrument (Figure 5a). When the sample had been tilted further, the cells were subsequently milled with the ion beam parallel to the substrate (Figure 5b). The cross-sectioning procedure produces a flat surface (Figure 5b and S3). The same cell is highlighted in Figures 5b and c, and the images also show small square etch marks made in the substrate by the FIB.

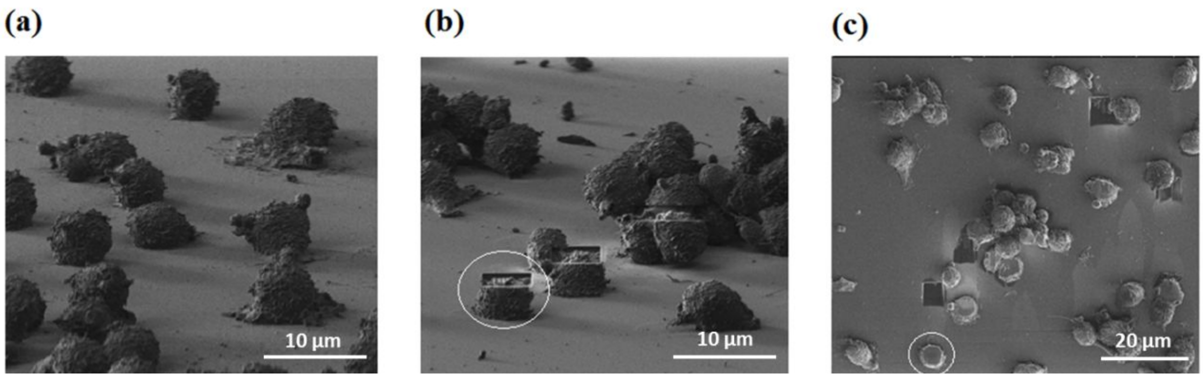

Figure 5: *(a) Microglial cells exposed to AgNWs supported on a silicon substrate, imaged in the FIB instrument in secondary electron mode before being cross sectioned. (b) The cells that have been cross-sectioned in the FIB in side view and (c) top view.*

Correlative SEM and ToF-SIMS ion imaging of exactly the same cross-sectioned cells was performed (Figure 6). Once again, the SIMS identified the general protein fragments (blue) and Ag^+ ions (red), but the signal from the sulfur-producing enzymes was weak (Figure 6b). The signal intensity appeared to be reduced, as a result of Ga^+ ion beam damage incurred during FIB cross-sectioning, even after cleaning with C_{60}^+ sputtering. The cells from FE-SEM could be correlated with the TOF-SIMS ion images, but the biological secondary ion signals were not strong in the SIMS ion map. During the FIB milling two factors reduce the ion beam induced damage in the cells: the samples are coated with a metallic layer before milling, and they are also orientated at high angle of incidence (~90°) in order to cross section the cells. At this high angle of incidence, the majority of ion beam damage occurs at the point where the beam hits the substrate. However, a small degree of damage will occur, as has been shown in samples fabricated for TEM analysis [ref]. The result of this damage is observed in the reduced secondary ion counts obtained from the FIB milled samples. Compared to the C_{60}^+ sputter cleaned samples, the secondary ion signal for the cystathionine fragments have dropped from 5.4×10^5 counts to 1.6×10^5 for the FIB milled cells. Conversely, there has been a slight increase in the smaller organic fragments from the FIB milled cells which indicate that larger molecules have been broken resulting in a greater number of smaller fragment ions. Much lower ion beam energies are needed to minimise this beam damage in order to reduce the loss of the larger organic molecules from the cells. If damage-free samples made via FIB cross-sectioning can be made that maintain the integrity of the larger organic molecules, then this approach may enable sub-cellular chemico-spatial mapping of internal cell. Thus, compositional variations through a cell could be measured without the need to depth profile through a cell from the top down, where changes in sputter rate and geometry cause problems in accurately associating chemical changes to depth.

Application of EDX mapping in the SEM, demonstrated that the silver (Figure 6d) was associated with a strong sulfur signal (Figure 6e), indicating that the AgNWs were sulfided within the cells. This transformation to crystalline Ag_2S NPs was confirmed using high resolution transmission electron microscopy (Figure S4). Taken together this work indicates the signal from the enzyme fragments was lost during FIB milling, but that that is was still possible to confirm the presence of silver from the AgNWs within the cell.

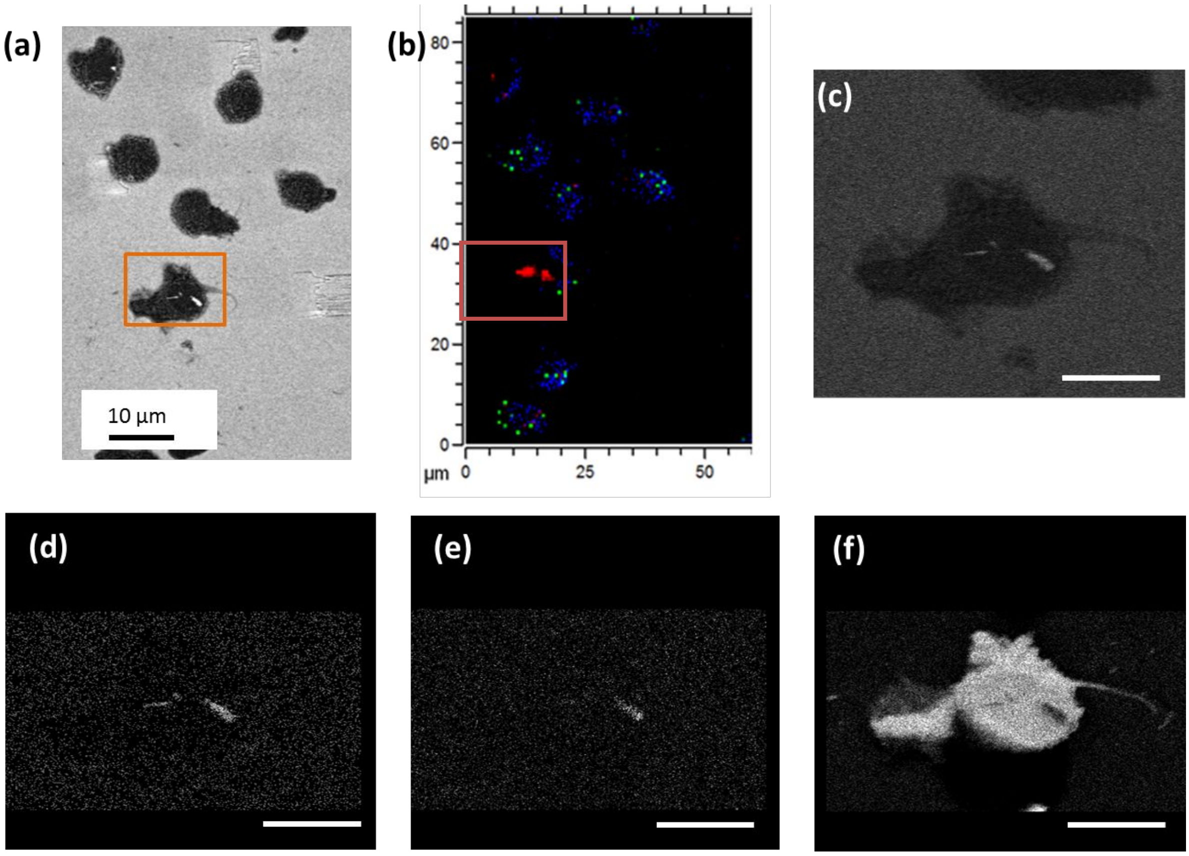

Figure 6: *(a) Cellular uptake of AgNWs in microglia imaged in SEM - BSE mode; (b) overlay SIMS image show signal intensities of* Ag^{+} *(red), the cystathionine,* $C_6H_{13}N_2O_4S^{+}$ *(green) and protein,* $C_4H_8N^{+}$ *(blue) fragment ions (c) SEM- BSE image of AgNWs (D= 70 nm; L= 1-4 µm) inside the boxed microglial cell in figure 6a,b and EDS mapping of (d) Ag* $L_{\alpha 1}$*, (e) S* $K_{\alpha 1}$ *and (f) C* $K_{\alpha 1}$ *(scale bar= 10 µm).*

Confocal microscopy and Western blotting

Finally, we benchmarked the TOF-SIMS technique against confocal microscopy images of fluorescently labelled antibodies against the sulfur producing enzymes, to confirm the presence of the hydrogen sulfide (H_2S) - synthesising enzymes after the microglia were treated with AgNWs. The expression of the H_2S-synthesizing enzymes cystathionine-γ-lyase (CSE), cystathionine β-synthase (CBS) and mercaptopyruvate sulfur transferase (MPST) were confirmed using confocal microscopy after the microglial cells had been pulsed for 1h with AgNWs followed by a 24h chase period (Figure S5a-f). In the confocal images, the expression level of all these H_2S producing enzymes (CBS, CSE and MPST) did not increase significantly (Figures S5c,f,i). Western blots (Figure S5j-l) also confirm that the sulfur-producing enzymes could be measured, but there was no significant upregulation of the CSE enzymes in N9 cells exposed to the silver AgNWs. These results contrast our previous work on the AgNPs, which did detect upregulation of these enzymes following cell exposure (Figures S5m). The measured differences between the AgNWs and AgNPs can possibly explained by the fact that the AgNWs are less soluble than the AgNPs, since their long axes are coated with PVP [17].

Effect of AgNW treatment on microglial cell activity

Finally, the effect of AgNWs-treatment on microglial cell viability, LPS-induced reactive oxygen species (ROS) production, TNFα release and nitrite production was assessed (Figure S6). AgNWs were not significantly toxic (measured by the LDH release and MTS assays) and did not show a dose-dependent toxicity at concentrations of 6.25 – 50 μg/mL after a 1 h pulse exposure and 24 h chase (Figure S6a,b). This finding correlates with our previous study, which demonstrates an AgNPs-detoxifying mechanism in microglia, involving the inhibition of oxidative dissolution by the sulfiding of the silver [9]. A similar AgNWs treatment (even at high dose up to 50 μg/mL) did not significantly affect pro-inflammatory cytokine (IL-6 and TNFα) release (Figure S6c-d). While there was a slight yet significant reduction in basal levels of ROS production by AgNW treatment, no effect on mitochondrial membrane potential was evidenced (Figure S6e,f). Treatment with LPS as a positive control led to a robust increase in production of TNFα, IL-6 and ROS (Figure S6c-e), with a concomitant decrease in mitochondrial membrane potential (Figure S6f), clearly demonstrating a shift towards a microglia inflammatory phenotype. Simultaneous treatment of microglia with LPS (500 ng/mL) and AgNWs led to a significant decrease in production of the inflammatory marker TNFα compared to LPS treatment alone (Figure S6g). While there was also a slight decrease in ROS and nitrite production following AgNW treatment (Figure S6h-i), this did not reach statistical significance.

CONCLUSIONS

Detection of enzymes without using labels is a fundamental challenge in the biological and medical sciences. Imaging ToF-SIMS is one of the few spatially resolved analytical techniques with the chemical specificity, surface sensitivity and spatial resolution to detect enzyme fragments within cells. This technique has been used widely in biomaterials research to characterise peptide/cellular attachment to biomaterials surfaces, and more recently, ToF-SIMS has also been successfully used to identify and spatially locate another unique S-containing metabolites in earth worm guts [18]. However, there are no reports to date that use this method to detect the colocation of enzymes in cells exposed to nanomaterials. During high resolution mass spectrometry of the C_{60}^+ ion beam cleaned cell surfaces, Ag^+ ion peaks were clearly seen in the positive ion spectrum in the cells containing the AgNWs; protein fragment ion signals of the amino acids ($C_4H_8N^+$), and fragments of cystathionine-γ-lyase. Other fragments from MPST ($C_2H_6OS^+$) and CBS ($C_2H_6O_2^+$) were also detected, but not to the same intensity as those observed from the cystathionine. These results confirm that ToF-SIMS is sufficiently sensitive to detect these sulfur-producing enzymes within cells and that these enzymes can be detected without the use of any labelling. To our knowledge this is the first time that these techniques have been used successfully to image enzymes inside cells, so we do not yet know the range of proteins that can be detected. Although detection of the signals was possible using the ToF-SIMS ion spectrometry mode, but due to poor mass resolution in the first instance and ion beam induced damage in the second, the secondary ion signal pertaining to the sulfur containing enzymes could not be imaged. The sectioning of the cells also showed that silver was present inside the cells, and not just on the surface of the cells. However, varying ionisation probabilities of the different molecules can be complicated, which means more thorough studies will be needed for absolute quantifications using current TOF-SIMS instrumentation, or clarification of any up regulation of these enzymes [19, 20].

In future, application of new Xe^+ plasma ion beams for cross sectioning, will cause less damage in the samples making it possible to generate spatially resolved SIMS maps of the cell cross sections [21]. Imaging with an ion beam that would enhance the secondary ion signal, such as oxygen, could also be preferential for improving the signal intensities. Investigating the interaction of silver nanomaterials (AgNMs) with proteins, enzymes or gaseous transmitter (*e.g.* H_2S) and their possible transformation within the cellular environment provides a better understanding of the mechanisms involved in any potential AgNMs neurotoxicity. This study paves the way for application of TOF-SIMS as a complementary characterisation tool to map the distribution of sulfur producing enzymes inside cells, their site of action inside the cells and their relative contributions. More generally the results highlight the promise of this technique for the label-free identification of other enzymes in a range of biological systems.

Methods

Silver Nanowires Synthesis and Characterisation

Silver nanowires (AgNWs) were prepared *via* a modified polyol pathway through the reduction of $AgNO_3$ with ethylene glycol in the presence of poly(vinyl pyrrolidone) (PVP; Sigma-Aldrich, UK). Ethylene Glycol (EG; Sigma-Aldrich, anhydrous, 99.8%; 5.5 mL) was placed in a double-neck round-bottom flask connected to a condenser. A stock solution of 0.05 M sodium chloride (NaCl) was prepared by dissolving NaCl in EG by sonication. The appropriate amount of NaCl stock solution was added to the flask so that the concentration of NaCl in the final reaction volume was 60 mM. The flask was heated in an oil bath at 160 °C, to remove trace amounts of water. Meanwhile, argon flow and magnetic stirring were applied and maintained throughout the synthesis. Silver nitrate ($AgNO_3$, 25 mM, Sigma-Aldrich, >99%) and PVP, with an average molecular weight $M_w \approx 360k$, were dissolved in 3.5L EG by magnetic stirring in the dark. The molar ratio of PVP to $AgNO_3$ was 1.5, where the concentrations of PVP were calculated in terms of the repeating unit. After 1 hour of heating of the reaction flask, 3 mL of the $AgNO_3$/PVP/EG solution were added drop-wise. After injection, the reaction mixture was refluxed at 160 °C and went through a number of colour changes until the mixture became stable at approximately 90 min. The reaction was quenched by cooling the flask in a room-temperature water bath. The reaction mixture was transferred to a centrifuge tube and diluted with acetone 5 times by volume. The AgNWs were collected by centrifugation at 4500 rpm for 10 min. The washing process was repeated with ethanol and deionized water, to ensure that most of the EG and PVP were removed. The sample was finally dispersed in 5 mL of deionised water. These purified AgNWs were sealed, stored in the dark and kept in a refrigerator. Full characterisation of the physicochemical properties of the PVP-coated AgNWs used in this study was previously reported by Chen *et al.*[22] and are summarized in Table S1.

Cell exposures and confocal microscopy

Microglia experiments were carried out on the immortalized embryonic mouse microglia N9 cell line, first developed by Dr. Ricciardi-Castagnoli *et al.* [23] and given as a kind gift by Dr. Deanna Taylor, Imperial College London. N9 microglia reliably replicate cultured primary microglia with respect to nitric oxide (NO) production, cytokine synthesis and expression of cell surface markers [24-26]. N9 microglia were cultured in

Dulbecco's Modified Eagle's medium (DMEM) with 5% Fetal Calf Serum (FCS), 8 mM L-glutamine and 50 U/mL Penicillin and 50 μg/mL streptomycin (termed full DMEM) at 37^{o}C in a humidified atmosphere with 5% CO_2. In this experiment, expression of H_2S producing enzymes (cystathionine-γ-lyase (CSE), cystathionine β-synthase (CBS) and mercaptopyruvate sulfurtransferase (MPST)) in microglia N9 cells were assessed following AgNWs treatment. N9 cells were seeded on round cover slips (13mm in diameter) in 24 well-plate for 24 h before the exposure. The cells were then washed with serum-free RPMI (with 8mM L-glutamine and 50 U/mL Penicillin and 50 μg/mL streptomycin; termed SF-RPMI) and incubated with AgNWs, 50 μg/ml in SF-RPMI for 1 h at 37^{o}C. The AgNW were then removed, and the cells incubated for a further hour in SF-RPMI, followed by a 23hr incubation in full DMEM before fixation using ice cold methanol. The cells were blocked (1% BSA in PBS, pH 7.4) for 30 mins before incubation with primary antibodies (1:200 dilution) at 4 °C overnight. The cells were next incubated with the fluorescent-labelled secondary antibodies (1:200 dilution) for 1 h at room temperature. Nuclei were counter stained with Hoechst 33342 (blue). The glass cover slips were mounted onto microscope slides with SlowFade® antifade reagent and visualized using a Leica SP5 inverted confocal microscope (Leica, Germany). Three separate experiments were performed with total number of 120 cells (40 cells per experiment) observed. The fluorescent intensity of the enzymes was measured using Fiji (Image J) analysis software and the data were expressed as mean fluorescent intensity showing the standard deviation.

TOF-SIMS Analysis of AgNWs Uptake by Microglial Cells

For TOF-SIMS analysis, the microglia cells (the control sample) and microglial cells exposed to the AgNWs (70 nm in diameter and 1.5 μm long) [27] were seeded on 13 mm diameter glass cover slips. Microglia cells were critically point dried (CPD) with liquid carbon dioxide after dehydrating with ethanol. To preserve sample morphology and chemistry using the CPD method, water was replaced by exchange fluids (*e.g.* ethanol or acetone) and in turn replacing the exchange fluid with liquid CO_2. Then, the liquid CO_2 converted to the gaseous phase at critical point (31 ºC; 74 bars) without changing density. Therefore, surface tension effects which may distort morphology and ultra-structure can be eliminated. The spectra and imaging data were acquired using a TOF-SIMS 5 instrument (ION-TOF, Germany) equipped with a bismuth primary ion source and a C_{60}^+ sputter ion source (at the time of the study the Ar_n^+ GCIB was not available).

The introduction of polyatomic ion beams, C_{60}^+ has been associated with relatively lower surface damage, improving detection limits, and enhanced efficiency of the analysis [28]. The increase in sputtered secondary ion species is because each atom within the C_{60} cluster carries a fraction of the total energy when an ion is accelerated and impacts the surface. For instance, in the case of C_{60}^+, there will be up to 60 separate collisions of approximately 250 eV, instead of a single particle with 15 keV bombarding the surface. This energy is deposited much closer to the surface and thus increases the sputter yield, leading to an increase in secondary ion yield [28]. Here, sputtering by C_{60}^+ was performed on a 500 µm x 500 µm area at energy of 10 keV for surface cleaning purposes. Selected peaks known to be protein fragments such as glycine (CH_4N^+) and alanine ($C_2H_6N^+$) were monitored, along with known peaks from PDMS at masses 73, 147, 207 and 221 amu. Once the PDMS peaks intensity had plateaued in the depth profile and the secondary ion count from the protein fragments were more resolved, the surface was deemed to be 'cleaned'. The 3D renders of the protein fragments shows how the cells become more resolved during the sputter-clean stage (see supporting information, figure S2) and the secondary ion yield from the samples is improved [29].. Recently the Ar_n^+ gas cluster ion beam has become more common for sputter depth profiling of polymeric and biological based samples, on the type of dual beam ToF-SIMS instruments used in this study.

The SIMS analysis consisted of a 'cleaning' sputter cycle of 0.5s with the C_{60}^+ ion beam with a current of 0.6nA, followed by the analytical scan, then a pause of 1s to reduce any charging on the surface. This sequence was then repeated until the analysis was deemed finished. Using a 25 keV Bi_3^+ primary ion beam an initial image is taken over an area of 300µm x 300µm with 512 x 512 pixels, in order to see the cleaned cells. The high resolution imaging is then carried out over an area of 100µm x 100µm with 512 x 512 pixels (~195nm/pixel)

Focused Ion Beam (FIB) and FIB-Secondary Electron Microscopy (SEM) - EDX

To map any co-localisation between the AgNWs and the sulfur producing enzymes inside the cells, the same cells were cross sectioned using a FIB instrument (FEI 200 TEM) and then analysed by energy-dispersive x-ray spectroscopy (EDX) in the SEM and also ion mapped in the ToF-SIMS.

Before beginning the FIB milling, the sample was coated with a metallic layer to protect against unwanted beam-damage. Specimen milling and imaging was conducted using a FIB-SEM-EDS system equipped with a Ga^+ ion source (Zeiss Auriga 40). The milling current of 2 nA, at 30 kV was selected in a Dual Beam system for FIB/SEM operation. Lower beam currents of 120 pA was used to polish the cross section. For imaging, the in-lens and backscattered (BSE) detectors as well as an X-ray analyser for EDX with an operating voltage of 20 kV were applied.

Statistical analysis

The data were analysed by one-way ANOVA with Tukey's *post-hoc* test using GraphPad Prism 7 software. Differences between means were considered statistically significant at $p < 0.05$. Data are presented as mean ± standard error of the mean (SEM) of at least three independent experiments, unless otherwise stated.

Supporting Information. The reader is referred to the Supporting Information Available online, which provides further details of material characterisation of Ag NWs, a negative polarity secondary-ion spectrum recorded from AgNWs in microglia cells after sputtering with C_{60}^+, TEM images showing Ag_2S NPs in microglial cells exposed to the AgNWs, confocal microscopy and western blotting data, and the cell viability assays. Tables showing the list of ligands which are found in the CBS, CSE and MPST enzyme structures are also provided.

AUTHOR INFORMATION

Corresponding Authors

*Alexandra E. Porter, a.porter@imperial.ac.uk and Mary P. Ryan, m.p.ryan@imperial.ac.uk

Author Contributions

BFL, DGC, KFC, PR, MPR and AEP designed the study. BFL, DGC, SF, PR, AEG, SC carried out the experiments. AEP, SF and BFL wrote the manuscript. All authors revised the manuscript.

Funding Sources

An ERC starting investigator grant to AEP (CNTBBB), and RAEng/Shell Research Chair to MPR. LBF acknowledges the financial support from University of Malaya research grant, UMRG (RP045D-17AET) and AEP/MPR acknowledge NERC grant NE/N006402/1.

REFERENCES

1. Whelan, D. R.; Lee, W. T. C.; Yin, Y. D.; Ofri, D. M.; Bermudez-Hernandez, K.; Keegan, S.; Fenyo, D.; Rothenberg, E., Spatiotemporal dynamics of homologous recombination repair at single collapsed replication forks. *Nature Communications* **2018,** *9*.
2. Youn, S. C.; Chen, L. Y.; Chiou, R. J.; Lai, T. J.; Liao, W. C.; Mai, F. D.; Chang, H. M., Comprehensive Application of Time-of-flight Secondary Ion Mass Spectrometry (TOF-SIMS) for Ionic Imaging and Bio-energetic Analysis of Club Drug-induced Cognitive Deficiency. *Scientific Reports* **2015,** *5*.
3. Kim, J. H.; Ahn, B. J.; Park, J. H.; Shon, H. K.; Yu, Y. S.; Moon, D. W.; Lee, T. G.; Kim, K. W., Label-free calcium imaging in ischemic retinal tissue by TOF-SIMS. *Biophysical Journal* **2008,** *94* (10), 4095-4102.
4. Tolbert, A. K.; Young, J. M.; Jung, S.; Chung, D.; Passian, A.; Westpheling, J.; Ragauskus, A. J., Surface Characterization of Populus during Caldicellulosiruptor bescii Growth by TOF-SIMS Analysis. *Acs Sustainable Chemistry & Engineering* **2017,** *5* (3), 2084-2089.
5. Goacher, R. E.; Edwards, E. A.; Yakunin, A. F.; Mims, C. A.; Master, E. R., Application of Time-of-Flight-Secondary Ion Mass Spectrometry for the Detection of Enzyme Activity on Solid Wood Substrates. *Analytical Chemistry* **2012,** *84* (10), 4443-4451.
6. Weng, N. Y.; Jiang, H. B.; Wang, W. X., In Situ Subcellular Imaging of Copper and Zinc in Contaminated Oysters Revealed by Nanoscale Secondary Ion Mass Spectrometry. *Environmental Science & Technology* **2017,** *51* (24), 14426-14435.
7. Urbini, M.; Petito, V.; de Notaristefani, F.; Scaldaferri, F.; Gasbarrini, A.; Tortora, L., ToF-SIMS and principal component analysis of lipids and amino acids from inflamed and dysplastic human colonic mucosa. *Analytical and Bioanalytical Chemistry* **2017,** *409* (26), 6097-6111.
8. Bluestein, B. M.; Morrish, F.; Graham, D. J.; Guenthoer, J.; Hockenbery, D.; Porter, P. L.; Gamble, L. J., An unsupervised MVA method to compare specific regions in human breast tumor tissue samples using ToF-SIMS. *Analyst* **2016,** *141* (6), 1947-1957.
9. Daniel, A. G.; Leo, B. F.; Pakatip, R.; Shu, C.; Angela, E. G.; Ioannis, G. T.; Raffaella, C.; Milo, S. P. S.; David, T. D.; Mary, P. R.; Alexandra, E. P., Silver nanoparticles reduce brain inflammation and related neurotoxicity through induction of H 2 S-synthesizing enzymes. *Scientific Report* **2017,** *7*.
10. Dufton, N.; Natividad, J.; Verdu, E. F.; Wallace, J. L., Hydrogen sulfide and resolution of acute inflammation: A comparative study utilizing a novel fluorescent probe. *Scientific Reports* **2012,** *2*.
11. Du, C.; Jin, M.; Hong, Y.; Li, Q.; Wang, X.-H.; Xu, J.-M.; Wang, F.; Zhang, Y.; Jia, J.; Liu, C.-F.; Hu, L.-F., Downregulation of cystathionine beta-synthase/hydrogen sulfide contributes to rotenone-induced microglia polarization toward M1 type. *Biochemical and Biophysical Research Communications* **2014,** *451* (2), 239-245.
12. Baker, M. J.; Zheng, L.; Winograd, N.; Lockyer, N. P.; Vickerman, J. C., Mass Spectral Imaging of Glycophospholipids, Cholesterol, and Glycophorin A in Model Cell Membranes. *Langmuir* **2008,** *24* (20), 11803-11810.
13. McLafferty, F. W.; style="margin-top:9.0pt, F. T. p. c. M.; margin-right:0cm; margin-bottom:0cm; margin-left:0cm; margin-bottom:.0001pt; line-height:normal">, *Interpretation Of Mass*

Spectra. University Science Books: 1993.
14. Boonrungsiman, S.; Fearn, S.; Gentleman, E.; Spillane, L.; Carzaniga, R.; McComb, D. W.; Stevens, M. M.; Porter, A. E., Correlative spectroscopy of silicates in mineralised nodules formed from osteoblasts. *Nanoscale* **2013,** *5* (16), 7544-7551.
15. Breitenstein, D.; Rommel, C. E.; Mollers, R.; Wegener, J.; Hagenhoff, B., The chemical composition of animal cells and their intracellular compartments reconstructed from 3D mass spectrometry. *Angewandte Chemie-International Edition* **2007,** *46* (28), 5332-5335.
16. Braun, R. M.; Beyder, A.; Xu, J. Y.; Wood, M. C.; Ewing, A. G.; Winograd, N., Spatially resolved detection of attomole quantities of organic molecules localized in picoliter vials using time-of-flight secondary ion mass spectrometry. *Analytical Chemistry* **1999,** *71* (16), 3318-3324.
17. Theodorou, I. G.; Muller, K. H.; Chen, S.; Goode, A. E.; Yufit, V.; Ryan, M. P.; Porter, A. E., Silver Nanowire Particle Reactivity with Human Monocyte-Derived Macrophage Cells: Intracellular Availability of Silver Governs Their Cytotoxicity. *Acs Biomaterials Science & Engineering* **2017,** *3* (10), 2336-2347.
18. Liebeke, M.; N.Strittmatter; S.Fearn; Morgan, A. J.; Kille, P.; Fuchser, J.; Wallis, D.; Palchykov, V.; J.; Robertson; Lahive, E.; Spurgeon, D. J.; D.McPhail; Z.Takats; Bundy, J. G., Uniques metabolites

protect earthworms against plant polyphenols. *Nature Comm.* **2015,** *6:7869*

19. Wittmaack, K., A UNIFIED EXPLANATION FOR SECONDARY-ION YIELDS AND MECHANISM OF THE SIMS MATRIX EFFECT - COMMENT. *Journal of Applied Physics* **1981,** *52* (1), 527-529.

20. Vickerman, J. C.; Briggs, D., *ToF-SIMS: Materials Analysis by Mass Spectrometry*. IM Publications, 2013: 2013.

21. Burnett, T. L.; Kelley, R.; Winiarski, B.; Contreras, L.; Daly, M.; Gholinia, A.; Burke, M. G.; Withers, P. J., Large volume serial section tomography by Xe Plasma FIB dual beam microscopy. *Ultramicroscopy* **2016,** *161*, 119-129.

22. Chen, S.; Goode, A. E.; Sweeney, S.; Theodorou, I. G.; Thorley, A. J.; Ruenraroengsak, P.; Chang, Y.; Gow, A.; Schwander, S.; Skepper, J.; Zhang, J.; Shaffer, M. S.; Chung, K. F.; Tetley, T. D.; Ryan, M. P.; Porter, A. E., Sulfidation of silver nanowires inside human alveolar epithelial cells: a potential detoxification mechanism. *Nanoscale* **2013,** *5* (20), 9839-9847.

23. Righi, M.; Mori, L.; Delibero, G.; Sironi, M.; Biondi, A.; Mantovani, A.; Donini, S. D.; Ricciardicastagnoli, P., MONOKINE PRODUCTION BY MICROGLIAL CELL CLONES. *European Journal of Immunology* **1989,** *19* (8), 1443-1448.

24. Bulgarelli, I.; Tamiazzo, L.; Bresciani, E.; Rapetti, D.; Caporali, S.; Lattuada, D.; Locatelli, V.; Torsello, A., Desacyl-ghrelin and Synthetic GH-secretagogues Modulate the Production of Inflammatory Cytokines in Mouse Microglia Cells Stimulated by beta-Amyloid Fibrils. *Journal of Neuroscience Research* **2009,** *87* (12), 2718-2727.

25. Bureau, G.; Longpre, F.; Martinoli, M. G., Resveratrol and quercetin, two natural polyphenols, reduce apoptotic neuronal cell death induced by neuroinflammation. *Journal of Neuroscience Research* **2008,** *86* (2), 403-410.

26. Chang, L. C.; Tsao, L. T.; Chang, C. S.; Chen, C. J.; Huang, L. J.; Kuo, S. C.; Lin, R. H.; Wang, J. P., Inhibition of nitric oxide production by the carbazole compound LCY-2-CHO via blockade of activator protein-1 and CCAAT/enhancer-binding protein activation in microglia. *Biochemical Pharmacology* **2008,** *76* (4), 507-519.

27. Chung, K. F.; Seiffert, J.; Chen, S.; Theodorou, I. G.; Goode, A. E.; Leo, B. F.; McGilvery, C. M.; Hussain, F.; Wiegman, C.; Rossios, C.; Zhu, J.; Gong, J. C.; Tariq, F.; Yufit, V.; Monteith, A. J.; Hashimoto, T.; Skepper, J. N.; Ryan, M. P.; Zhang, J. F.; Tetley, T. D.; Porter, A. E., Inactivation, Clearance, and Functional Effects of Lung-Instilled Short and Long Silver Nanowires in Rats. *Acs Nano* **2017,** *11* (3), 2652-2664.

28. Jones, E. A.; Fletcher, J. S.; Thompson, C. E.; Jackson, D. A.; Lockyer, N. P.; Vickerman, J. C., ToF-SIMS analysis of bio-systems: Are polyatomic primary ions the solution? *Applied Surface Science* **2006,** *252* (19), 6844-6854.

29. Weibel, D.; Wong, S.; Lockyer, N.; Blenkinsopp, P.; Hill, R.; Vickerman, J. C., A C-60 primary ion beam system for time of flight secondary ion mass spectrometry: Its development and secondary ion yield characteristics. *Analytical Chemistry* **2003,** *75* (7), 1754-1764.